



# Understanding the anticorrosion properties of chitosan grafted poly-aspartic acid against mild steel corrosion in 1 M HCl: Electrochemical and theoretical considerations

Annuncieta C. Njoku<sup>1</sup>, Placid I. Anyanwu<sup>1\*</sup>, Simeon C. Nwanonyi<sup>1,\*\*</sup>

<sup>1</sup>Department of Polymer & Textile Engineering, Federal University of Technology Owerri, P.M.B. 1526 Owerri, Imo State, Nigeria

\*Corresponding author, Email address: [pianyanwu@gmail.com](mailto:pianyanwu@gmail.com)

\*\*Corresponding author, Email address: [nwanonyi.simeon@futo.edu.ng](mailto:nwanonyi.simeon@futo.edu.ng)

Received 09 Aug 2023,

Revised 31 Aug 2023,

Accepted 01 Sept 2023

**Citation:** Annuncieta C. Njoku., Placid I. Anyanwu Simeon C. Nwanonyi O. (2023) The understanding the anti-corrosion properties of chitosan grafted poly-aspartic acid against mild steel corrosion in 1 M HCl: characterization, electrochemical and theoretical considerations, *Mor. J. Chem.*, 11(4), 1183-1202

**Abstract:** The mechanism of the anticorrosion effects of chitosan grafted with poly-aspartic acid (CTS-PAA) against mild steel in 1 M HCl has been provided using combined electrochemical and theoretical approaches. The successful grafting of chitosan (CTS) with poly-aspartic acid (PAA) was verified with intensive Fourier-transformed infrared spectroscopy (FTIR). In the studied system, a minimal corrosion inhibition efficiency of about 60 % was obtained with the unmodified CTS whereas CTS-PAA inhibition efficiency reaching a maximum number of 98.9 % at 250 ppm concentration was obtained. Polarization studies show that the inhibitors acted on both the anodic and cathodic currents curves indicating a mixed inhibition protection mechanism while the electrochemical impedance data show that the protection was afforded by interfacial adsorption of the inhibitor species on the steel surface. The adsorption process fitted to Langmuir adsorption isotherm. The proposed inhibition mechanism linked the enhanced inhibition performance of CTS-PAA to the extension of the adsorption sites by the grafting agents which was confirmed with X-ray photoelectron spectroscopy (XPS) results. The experimental data were correctly complemented with density functional theory (DFT)/molecular dynamic simulation (MDS) data and the binding energy of the modified polymer is over two magnitudes higher than the individual molecules affirming the experimental findings.

**Keywords:** Intra-synergism; Impedance Spectroscopy; Surface Imagine; XPS; DFT; Monte Carlo

## 1. Introduction

Mild steel continues to find application in a wide area of industries owing to its low cost, mechanical resilience, and availability (Khodair *et al.*, 2019; Oguzie *et al.*, 2012). But the various steel cleaning processes such as pickling, descaling, etc., and other industrial activities like oil-well acidizing often involved acids and high temperatures (Khoshnaw and Gubner, 2022; Li and Celis, 2004). These aggravate the corrosion of steel (Khoshnaw and Gubner, 2022). And the aftermath of acid corrosion includes the loss of mechanical strength leading to the collapse and failure of oil pipelines, bridges, buildings, and leakage of chemical plants (Speight, 2014), etc. Several industries have come to understand that lack of management towards corrosion can be very costly and lead to material wastage but proper corrosion management leads to significant cost savings over the lifetime of an asset. Hence,

amongst the existing corrosion management/protection strategies including cathodic/anodic protections, alloying, surface coatings, etc., the use of corrosion-inhibiting additives is the most economical and versatile method to combat corrosion in diverse environments (Njoku *et al.*, 2021b; Oguzie *et al.*, 2014). In this regard, researchers from different backgrounds have proposed the use of different kinds of additives ranging from inorganic agents (Vaghefinazari *et al.*, 2022), organic/polymeric (Finšgar and Jackson, 2014; Verma *et al.*, 2022; Yihang, 2022), natural (Elmsellem *et al.*, 2014; Njoku *et al.*, 2018; Njoku *et al.*, 2019; Oguzie *et al.*, 2014; Wei *et al.*, 2020), and all sorts of synthetic compounds (Ouafi *et al.*, 2014; Chen *et al.*, 2022; Chopda, 2023). The restrictions on the use of many compounds especially chromate-based inorganic additives have encouraged the exploration of organic agents for corrosion protection (Vaghefinazari *et al.*, 2022). Also, the synthesis process of many synthetic compounds leaves lots of negative footprints on the environment (Sweetman, 2020). Considering the campaigns by several environmental agencies, presently researchers are considering the use of biodegradable and eco-friendly additives as corrosion inhibitors (Ani *et al.*, 2022; Natarajan and Zahir Said Al Shibli, 2021). Biopolymers are naturally derived polymeric compounds which are biodegradable, eco-friendly, and cheap when compared to inorganic, synthetic organic/polymeric compounds counterparts (Ananthi *et al.*, 2021; Shahini *et al.*, 2021). Biopolymers possess the advantage of high chelating ability and large molecular size which enhance the surface coverage of the metal surface (Nascimento *et al.*, 2023; Verma and Quraishi, 2021). In this regard, polymeric inhibitors from natural sources have been reported as a potential alternative for acid corrosion due to their biodegradability, low cost, and effectiveness. For instance, natural polymers such as chitosan (Verma *et al.*, 2018), sodium alginate (Dang *et al.*, 2015; Wang *et al.*, 2023), glucose (Verma *et al.*, 2017), Arabic gum (El Azzouzi *et al.*, 2022), hydroxypropyl cellulose (Nwanonyi *et al.*, 2019), hyaluronic acid (Zhou *et al.*, 2020), carboxymethyl cellulose (Umoren *et al.*, 2018), etc., have been studied as benign corrosion inhibiting agents in varied media. But due to the limited heteroatoms and conjugated double bonds in the many polymer chains, the structural modification of these polymers with a variety of compounds to improve their overall anti-corrosion performance is a priority area. One prevailing approach to achieve this is the grafting of smaller molecules with heteroatoms like N, P, O, etc... (Erna *et al.*, 2019; Kong *et al.*, 2019). Heteroatoms are the sites of adsorption of organic molecules on metal. This is often achieved by donating the lone pairs of electrons to the vacant orbitals on the metal atoms. In this regard, several natural polymers such as chitosan, alginate, and gelatin lignin, etc., have been modified with small organic molecules with extensive heteroatoms and/or heterocyclic rings such as cinnamaldehyde polyamine (El Mouaden *et al.*, 2018), dopamine (Chai *et al.*, 2020), polyurethane (Abu Rub *et al.*, 2023), methyl acrylate (Auepattana-Aumrung *et al.*, 2022), 8-hydroxyquinoline (Fardioui *et al.*, 2021), acetylthiourea (Fekry and Mohamed, 2010), N-(2-hydroxy-3-trimethyl ammonium)propyl (Sangeetha *et al.*, 2015) etc. In these reports, the adsorption sites and corrosion inhibition of the natural polymers were improved. Similarly, the present investigation employed glutaraldehyde as an imine bond linking agent to graft chitosan with polyaspartic and studied the improved corrosion-inhibiting ability against mild steel in 1 M HCl. The corrosion protection efficacies of the individual compounds (chitosan and polyaspartic acid) were minimal compared to the grafted polymer (CTS-PAA) which was the motivation for the grafting – a process best described as intra-synergism. The synthesis characterization was achieved with FTIR, while the corrosion inhibition ability was ascertained with combined gravimetric and electrochemical methods. XPS and SEM were employed to reveal the adsorption mechanism and microscopic protection, respectively. The proposed inhibition following experimental data was validated with vigorous DFT (density functional theory calculations) and molecular dynamics

simulation (MDS). The results presented here are quite innovative to the previous report on chitosan polyaspartic acid complex by providing a detailed mechanism that was supported by intensive complementing spectroscopic and computational approaches.

## 2. Methodology

### 2.1. Materials preparation

The metal substrate (mild steel) was cut into square coupons with dimensions: 5cmx5cmx0.1cm (for weight loss experiments) and 1cmx1cmx0.1cm (for electrochemical tests). In both experiments, the coupon samples were polished with Emery papers of different grits (150, 220, and 1000 grits) before experiments. Chitosan with a degree of acetylation of about 80, poly-aspartic acid, and glutaraldehyde (supplied by Sinopharm Chemical Reagent Co., Ltd) were used for the polymer grafting synthesis.

### 2.2 The grafting of chitosan with poly-aspartic Acid

The procedure is consistent with a slightly modified previous completing method technique (Chen et al., 2018). Chitosan powder (2g) was dissolved via continuous stirring with a magnetic stirrer at 30 °C in about 300 ml solution comprising a mixture of 2 % HCl solution and 5 % acetic acid. Then an equal volume of poly-aspartic acid (approx. 3 g/l) was added followed by the addition of about 4 ml of 40% glutaraldehyde at 40 °C and pH approx., 6.5. After the polymer precipitated in the presence of absolute ethanol solution, it was oven dried at the temperature of 40 °C overnight. The simplified reaction step is summarized in the scheme in Figure 1.

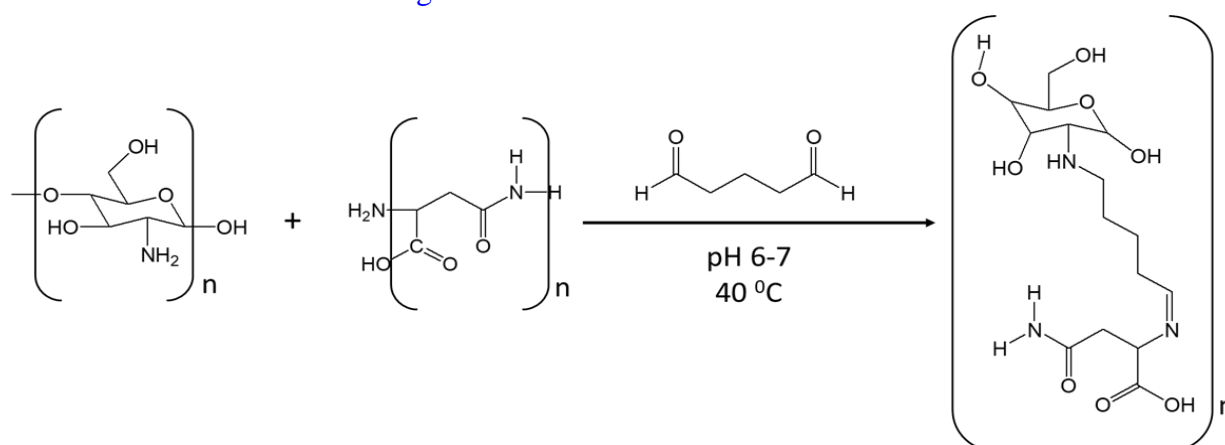


**Figure 1** Mechanism of the grafting of CTS with PAA.

### 2.3 Fourier-Transform Infrared Spectroscopy (FTIR)

This was used to characterize the synthesized chitosan grafted polyaspartic acid (CTS-PAA) by comparing it with the spectrum of polyaspartic acid (PAA) and chitosan (CTS). FTIR spectra were measured with ALPHA JCC ATR-FTIR equipped with OPUS software which extended from 400 - 4000  $\text{cm}^{-1}$ .

### 2.4 Weight loss experiments

Immersion tests were undertaken in 250 ml of unstirred test solutions at a temperature of ~298 K. The polished and reweighed steel samples coupons were submerged in beakers containing the test solutions using threads. To estimate the weight loss over time, test steel samples were retrieved at pre-determined time intervals of 24 hrs, 72hrs, 120hrs, and 168 h at room temperature, progressively washed with distilled water, and ethanol, then dried in warm air (using a hand dryer) before reweighing. The mass loss was calculated by subtracting the initial weight from the final weight. This was ascertained with a

digital weighing balance of 0.001 digits. Means of multiple measurements with low standard deviation ranging from 0.000 - 0.01 g/dm<sup>2</sup>.

## 2.5. Electrochemical measurements

The electrochemical results were obtained within a three-electrode corrosion cell by ZENNIUM XC complete dc voltammetry corrosion system with a ZAHNER analyzer. A sheet of platinum functioned the counter electrode while SCE (saturated calomel electrode) functioned as the RE (reference electrode). Electrochemical impedance spectroscopy (EIS) measurement was performed at the end of 1 h at  $25 \pm 2^\circ\text{C}$  against the reference electrode. Electrochemical impedance spectroscopy analysis was analyzed at  $E_{\text{corr}}$  (Corr. Potent.), at frequency ranges of 100 KHz-0.1 Hz and amplitude perturbation signal of 10 mV. Polarization (PDP) analysis was performed at a potential range of  $\pm 250$  mV against  $E_{\text{corr}}$ , with scan rate of 0.3333 mVs<sup>-1</sup> at  $25 \pm 2^\circ\text{C}$ . In both techniques, the results were monitored and extracted from the computer with the help of the earlier-mentioned software. Duplicate to triplicate data were recorded to confirm reproducibility.

## 2.6. Surface film analysis and morphological imaging

XPS was used to compare the sort of chemical interactions between CTS and CTS-PAA on the mild steel surface in 1 M HCl (XPS, ESCALAB 250) via apprising the binding energies of the distinct chemical bonds. SEM revealed the protection effect of the various inhibitors at the micro-scale level. The XPS analysis was conducted under pressures of approximately  $5.5 \times 10^{-8}$  mbar with Al K $\alpha$  (1486.6 eV). The binding energy profile fitting of the XPS data was achieved with the help of XPSPEAK Version 4.1 and standard carbon binding energy of 284.8 eV served as the reference value. A scanning electron microscope (SEM-INSPECT F50 model) was used for the imaging.

## 2.7. Computational details

Theoretical quantum chemical computations were performed in the framework of density functional theory (DFT) electronic structure programs as contained in material studio 7.0 software to determine the inhibitor effectiveness at the molecular level. In performing the calculations, the electronic structure of the inhibitors and iron (Fe) surface were modeled using DFT electronic structure programs- DMol3. Restricted spin polarization using the DNP basis set and Perdew Wang (PW) local correlation density function were also electronic parameters for the simulation. The electronic properties including HOMO, LUMO, and Fukui functions for electrophilic (F<sup>-</sup>) and nucleophilic (F<sup>+</sup>) attack and total electron density were determined. Local reactivity of the inhibitor molecules was assessed from Fukui indices (FI) to establish the adsorption centers or active centers through which the inhibitor molecules would likely interact with the Fe surface. Molecular dynamics (MD) simulation was performed using Forcite quench molecular dynamics to sample many different low-energy configurations and identify the low-energy minima of the non-covalent interaction between the inhibitor molecules and Fe surface. The calculations were done using a compass force field and a Smart algorithm. The overall protocol is consistent with our previous reports (Nwanonyi *et al.*, 2022)

# 3. Results and Discussion

## 3.1 Characterization of the synthesized inhibitor compounds

Figure 2 presented the FTIR spectra comparing the spectrum of (a) CTS and PAA (inset), and (b) CTS-PAA. The spectrum for CTS in Figure 2 (a) showed a stretching vibration band in the range of 3500–1000 cm<sup>-1</sup> corresponding to NH (primary and secondary) and OH or the intramolecular hydrogen bonds (Queiroz *et al.*, 2015). The peak at 1624 cm<sup>-1</sup> could be linked to the stretching of C–N vibration

and OH group by bonding (Wolkers *et al.*, 2004), while the adsorption band at  $1377\text{ cm}^{-1}$  represents the C–O stretching of primary alcohol group. The bands at  $1100$ ,  $1060$  and  $1024\text{ cm}^{-1}$  indicate the presence C–O stretching of polysaccharide bond (Lim and Hudson, 2004; Wolkers *et al.*, 2004). The N-acetyl residual groups typical to chitosan  $1665\text{ cm}^{-1}$  (C=O stretching of amide I) is obvious. The C–H symmetric and asymmetric stretching can be seen  $2921$  and  $2877\text{ cm}^{-1}$  absorption bands at around, respectively. These functional groups are typical of polysaccharide (Melo-Silveira *et al.*, 2012) such the carrageenans (Silva *et al.*, 2010) and glucans (Wolkers *et al.*, 2004). The small band around  $1550\text{ cm}^{-1}$  corresponds to N–H bending of amide II (Lim and Hudson, 2004). The peaks for  $\text{CH}_2$  bending and  $\text{CH}_3$  symmetrical deformations can be seen at  $1423$  and  $1375\text{ cm}^{-1}$ . The band around  $1153\text{ cm}^{-1}$  can be ascribed to the asymmetric stretching of the C–O–C Bridge (Vino *et al.*, 2012). All bands have been previously identified in the spectra of samples of chitosan reported by others (Song *et al.*, 2013; VINO *et al.*, 2012). PAA FTIR spectrum (Figure 2a-inset) reveals characteristic peaks at  $3420$  and  $1601\text{ cm}^{-1}$ , which can be ascribed to the stretching and bending vibrations of N–H in amide (Chen *et al.*, 2018). The peak at  $1,610\text{ cm}^{-1}$  is due to C=O of the carboxylic acid, while the peak at  $1398\text{ cm}^{-1}$  corresponds to the strong signal of C–N (Liu *et al.*, 2011; Njoku *et al.*, 2021a). The broad adsorption band around  $3100 - 3600\text{ cm}^{-1}$  is due to the stretching vibration of O–H (Wang *et al.*, 2017). The peak around  $1666$  and  $1601\text{ cm}^{-1}$  indicate –COOH and –CONH (Liu *et al.*, 2011). The peak for C–N is included in the  $1400\text{ cm}^{-1}$ . These peaks are consistent with previous data from the literature for PAA (Gao *et al.*, 2010; Huang and Kong, 2013). The combination of PAA and CTS can be verified from the FTIR of the grafted compound (PAA–CTS) shown in Figure 2b. Inspection of the plots reveals many peaks typical to CTS and PAA in the PAA–CTS. But some few peaks diapered while some new peaks appeared indicating a chemical reaction leading to the formation of new bonds. For instance, the peak at  $1589\text{ cm}^{-1}$  of the primary amine became weak, which indicates that amino group of CTS has been partly substituted by the imine bond. The above FTIR analysis shows the successful grafting of PAA with CTS in the CTS-PAA spectrum as illustrated in Figure 1 (Kumar *et al.*, 2012).

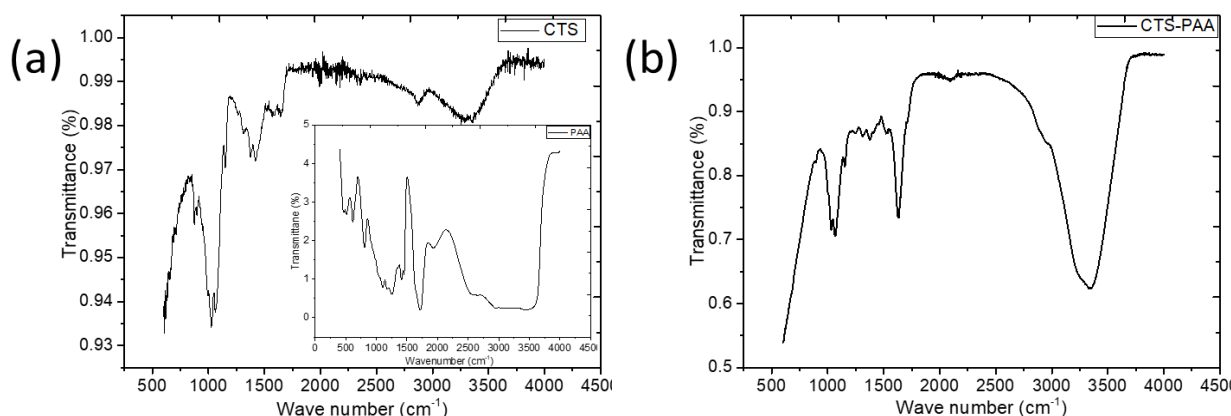


**Figure 2** FTIR spectra comparing the peaks of (a) CTS and PAA (inset), and (b) CTS-PAA

## 3.2 Anticorrosion testing

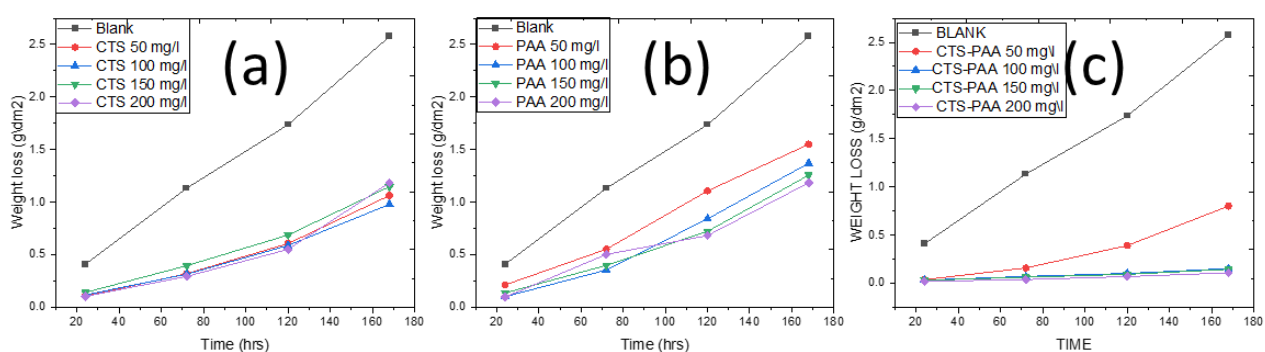
### 3.2.1 Gravimetric data

Figure 3 (a-c) illustrates the average weight loss for mild steel in 1 M HCl in the absence and presence of different concentrations of CTA, PAA, and CT-PAA, while Figure 4 (a-c) showed the corresponding inhibition efficiency values. Inspection of the results showed that the weight loss data in the absence of inhibitors were high, whereas in the presence of inhibitors minimal weight loss data was recorded. The weight loss reduction capacity decreases in the order CTS-PAA > CTS > PAA. This indicates that

the grafted CTS-PAA exhibited better protection ability than the individual PAA and CTS. The quantitative evaluation of the corrosion inhibition efficiency (IE%) of the various additives was achieved by adopting the model:

$$IE \% \left( 1 - \frac{W_{Inh}}{W_{blank}} \right) \times 100 \quad \text{Equ. 1}$$

Where,  $W_{Inh}$  and  $W_{blank}$  represent the weight losses obtained with and without the inhibitors. The plot of IE versus time for the various additives is presented in Figure 4 (a-c). The inhibition efficiency follows a surprising trend whereby the IE% versus time for CTS and PAA decrease with increasing time while the inhibition efficiency of the modified chitosan (CTS-PAA) slightly increases with time in the first half of the total time and maintained near-stable values over the whole exposure time (except at the lowest concentration). Very few additives pose this capability which indicates that the modified polymer (CTS-PAA) is an excellent inhibitor for steel in an acidic system.



**Figure 3** Weigh loss over time for mild steel in 1 M HCl in the presence and absence of CTS (a), PAA (b) and CTS-PAA (c)

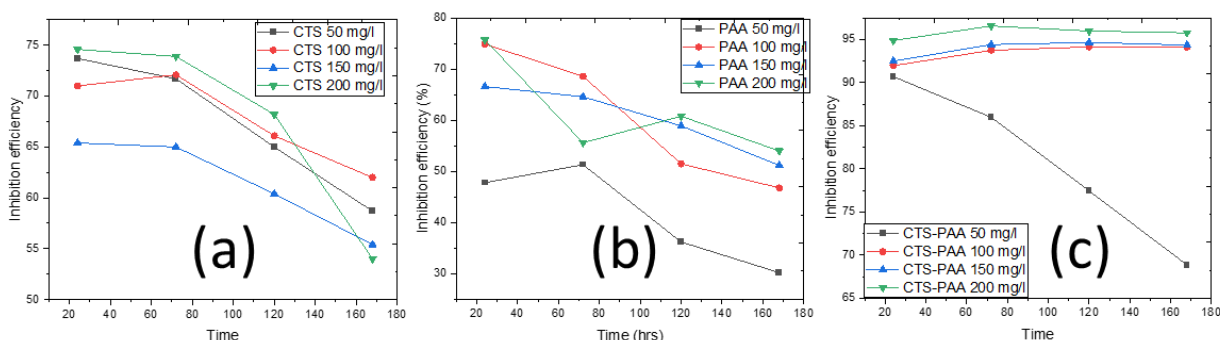


**Figure 4.** Plot of inhibition efficiency against time for mild steel corrosion in 1 M HCl in the presence of different concentrations of CTS (a), PAA (b) CTS-PAA (c).

### 3.2.2 Electrochemical data

#### 3.2.2.1 Potentiodynamic polarization

To corroborate the vigorous gravimetric data, electrochemical experiments were carried out utilizing the minimal and optimum concentrations of the various inhibitors. Consistently, the polarization tests were underrun provide evaluate the effects of CTS, PAA, and CTS-PAA on the anodic and cathodic corrosion processes. Representative polarization curves for the studied mild steel in 1 M HCl solution without and with different concentrations of the CTS, PAA, and CTS-PAA are shown in Figure 5 (a-c), respectively. Scrutiny of the polarization curves indicates that the introduction of the different

inhibitors shifts  $E_{\text{corr}}$  towards more negative values (in a concentration-dependent manner), as well as reducing both the anodic (slightly) and cathodic (pronouncedly) current densities. This suggests a mixed-type inhibition mechanism (Shanmugapriya *et al.*, 2023). The values of the current densities in the absence and presence of the different compounds were calculated from the extrapolation of the linear segments of the cathodic and anodic current arms following the existing model (Njoku *et al.*, 2019; Shanmugapriya *et al.*, 2023):

$$IE\% = \left(1 - \frac{i_{\text{corr,inh}}}{i_{\text{corr,0}}}\right) \times 100 \quad \text{Equ. 2}$$

Where,  $i_{\text{corr,inh}}$  and  $i_{\text{corr,0}}$  are the corrosion current densities with and without the inhibitors, respectively. From the polarization values presented in Table 1, it is conspicuous that although chitosan exhibited good anticorrosion efficacy at both low (50 mg/l) and high (250 mg/l) concentrations, the modified polymer – the CTS-PAA extensively improved the inhibition efficiency of >90, which is over a magnitude greater than CTS and PAA individual compounds. This can be attributed to intra-specific synergism between CTS and PAA.

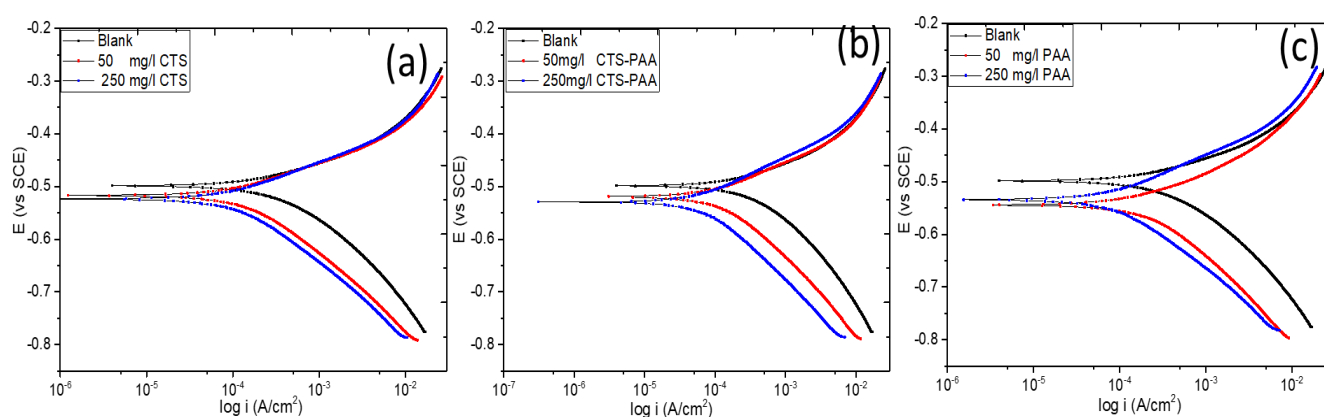


**Figure 5.** Potentiodynamic polarization curves mild steel in 1 M HCl without and with different concentrations of CTS (a), PAA (b) and the modified CTS (CTS—PAA) (c)

**Table 1** Polarization fitting data comparing the electrochemical results of mild steel in 1 M HCl without and with different concentrations of CTS, PAA and the modified CTS (CTS—PAA).

System	$E_{\text{coor}}$ (V vs SCE)	$I_{\text{coor}}$ ( $\mu\text{A}/\text{cm}^2$ )	IE%
Blank	-0.4937	342	-
CTS 100 mg/l	-0.5154	144	58
CTS 250 mg/l	-0.5179	109	68
PAA 50 mg/l	-0.5221	100	71
PAA 250 mg/l	-0.5314	91	73
CTS-PAA 50 mg/l	-0.5356	106	69
CTS-PAA 250 mg/l	-0.5440	55	84

PAA which is a smaller polymer in terms of mass with N heteroatom surprisingly showed lower inhibition values (even in the gravimetric data) which can be ascribed to the instability effects of the inhibitor in the aggressive acidic solution. But its grafting into chitosan polymer improved the overall anticorrosion efficacy of chitosan indicating enhancement of the interactive sites on CTS by the PAA or simply additional heteroatoms which constitute the adsorption sites in inhibiting species (Chauhan

*et al.*, 2019). This is often observed when smaller molecules with extensive heteroatoms are used to functionalize or modified natural polymers (Chauhan *et al.*, 2019; Chen *et al.*, 2018).

### 3.2.2.2 Electrochemical impedance spectroscopy (EIS)

EIS data provide information on the resistance to interfacial electron transfer as well as the influence of adsorbed species on this process. Figure 6 (a-c) shows the Nyquist plots comparing the impedance response of mild steel in 1 M HCl in the presence and absence varied amounts of CTS, PAA, and CTS-PAA. The various Nyquist plots are composed of conspicuous high frequency depressed capacitive semicircle with minor low frequency capacitive loop. The depressed semicircle is characteristic to solid electrodes that usually exhibit frequency dispersion (Njoku *et al.*, 2018; Oguzie *et al.*, 2014). The capacitive loop is analogous to the process of charge transfer coupled with the double layer capacitance effect. The diameter of the capacitive loop is a reflection of the charge transfer resistance ( $R_{ct}$ ). The magnitude of the charge transfer resistances at both the film and electrode surfaces ( $R_{ct1}$  and  $R_{ct2}$ ) for the mild steel specimen in 1 M HCl improved appreciably in the presence of the different inhibitors in a concentration-dependent manner but the modified polymer (CTS-PAA) showed higher values. The impedance fitting of the impedance results was executed with Zswimp software using equivalent circuit model  $R_s(Q_1(R_{ct1}(Q_2R_{ct2})))$  as shown in Figure 7. The fitting showed minimal error ( $\chi^2 = 1.0 \times 10^{-3} - 4.0 \times 10^{-4}$ ). The  $R_s$  component of the equivalent circuit denotes the solution resistance,  $R_{ct2}$  denotes the charge transfer resistance at the outer Helmholtz plan,  $R_{ct1}$  represents the interfacial film resistance;  $CPE_2$  ( $Q_2$ ) and  $CPE_1$  ( $Q_1$ ) are the double layer and film capacitive components of the constant phase elements (Nwanonyi *et al.*, 2022; Yaagoob *et al.*, 2023).

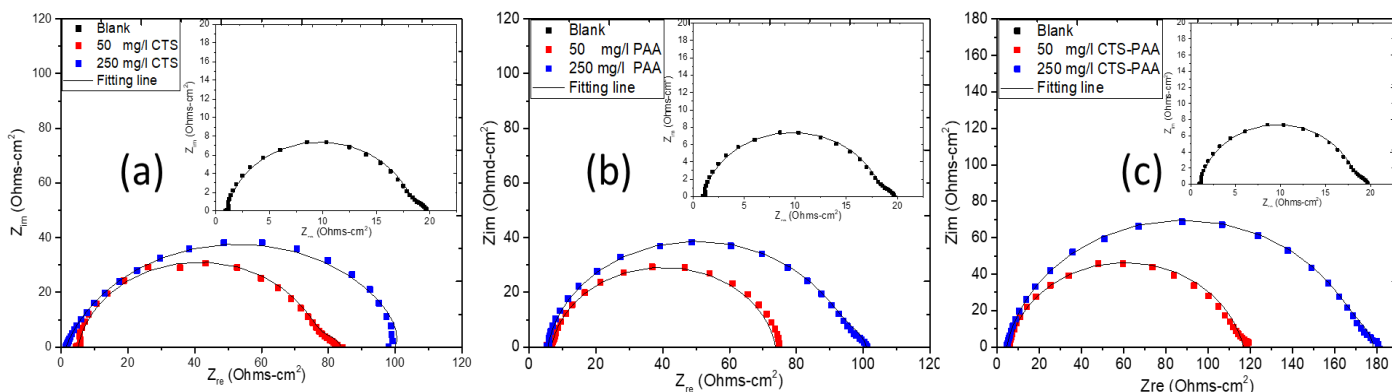


**Figure 6.** Nyquist impedance plots comparing the electrochemical results of mild steel in 1 M HCl without and with different concentrations of CTS (a), PAA (b) and the modified CTS (CTS-PAA) (c)

The results of the fitting are contained in Table 2. The  $n$  is a factor of the inhomogeneity of the interface while  $R_T$  is the sum of the charge transfer components athwart the double layer and the adsorbed film.  $R_T$  values were estimated as follows:  $R_T = R_{ct1} + R_{ct2}$  (and  $R_{ct1}$  and  $R_{ct2}$  are charge transfer resistances of the film and electrode surfaces respectively). The efficacy of inhibition ( $IE\%$ ) was ascertained from the  $R_T$  values for blank system ( $R_{T,blk}$ ) and for system containing the distinct inhibitors  $R_{T,inh}$  in accordance with the equation 3 and the values are included in Table 2:

$$IE \% = \left( \frac{R_{T,inh} - R_{T,blk}}{R_{T,inh}} \right) \times 100 \quad \text{Equ. 3}$$

A close look at the results in Table 2, it is two obvious that the introduction of different inhibitors caused the increase in the  $R_T$  values and the decrease in CPE values. The increase in  $R_T$  values is an



indication of the corrosion-inhibiting effect due to the adsorption of inhibitor films on the steel interface. Such a film can restrict the ingress of corrosive electrolytes ( $\text{Cl}^-$  and  $\text{H}^+$ ) (Onyeachu *et al.*, 2023). The decrease in CPE values is ascribed to the reduction in dielectric constants and/or an increase in the electric double-layer thickness at the interface, both of which are indicators of the replacement of adsorbed water molecules by inhibiting species (Emori *et al.*, 2023). Here again, the trend of the inhibition efficiencies agrees with the gravimetric and polarization data. PAA exhibited weak values compared to CTS, while CTS-PAA exhibits the best inhibition efficacy. CTS-PAA, therefore, presents a better choice for corrosion protection of mild steel in 1 M HCl than either chitosan (natural polymer) or the nontoxic polymer (PAA). EIS confirmed that the inhibitors could be adsorbed on the electrolyte/steel interface to achieve protection since double-layer capacitance values appreciably decreased in the inhabited systems.

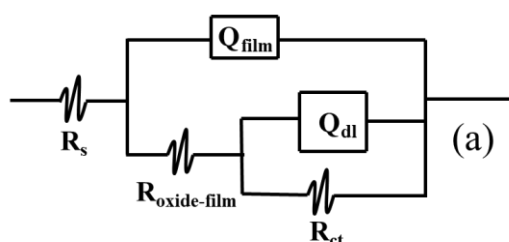


**Figure 7** The equivalent circuit model used in fitting the impedance results for mild steel in 1 M HCl without and with different concentrations of inhibitors.

**Table 2** Electrochemical parameters comparing the impedance data for steel in 1 M HCl, CTS, PAA and the modified CTS (CTS-PAA).

System	$R_s$ (Ohms-cm <sup>2</sup> )	CPE1 $Y_0$ ( $\pi Fcm^{-2}s^{n-1}$ )	n	Rct1 (Ohms-cm <sup>2</sup> )	CPE1 $Y_0$ ( $\pi Fcm^{-2}s^{n-1}$ )	n2	Rct2 (Ohms-cm <sup>2</sup> )	Rct <sub>T</sub> (Ohms-cm <sup>2</sup> )	IE	$X^2$ $\times 10^{-3}$
Blank	1.045	526	0.8982	17.4	216800	0.9348	1.4	19	-	
50 mg/l CTS	5.1	122	0.942	72	62230	0.7968	6.0	78	75.6	
250 mg/l CTS	1.4	60	0.8127	96.2	9924	1	1.6	98	81	1.1
50 mg/l PAA	5.5	12.5	0.9059	1.7	72.9	0.9133	66.5	68	72	1.3
250 mg/l PAA	5.6	10.7	0.9109	89	2829	0.8531	6.5	96	80	1.5
50 mg/l CTS-PAA	5.619	22.7	1	1.9	88.6	0.8139	109.1	111	83	1.7
250 mg/l CTS-PAA	4.462	88	0.8833	168	2881	1	6.0	174	89	0.4

### 3.4 Surface analysis

#### 3.4.1 Langmuir adsorption isotherm.

Adsorption isotherm fitting can be employed to establish that the corrosion inhibition exhibited by an organic compound is actually due to the adsorption of the molecules on the substrate. Langmuir adsorption isotherm provides the optimal regression. In this plot, the relationship between the degree of surface coverage ( $\theta$ ) ( $\text{IE}\% = \theta \times 100$ ) and the inhibitor concentration (expressed in mg/l) were employed to fit the gravimetric experimental data to the Langmuir adsorption isotherm model (Ouici *et al.*, 2016; Saha *et al.*, 2016):

$$\frac{C}{\theta} = \frac{1}{K} + C \quad \text{Equ. 4}$$

Where  $K$  is the equilibrium constant of the adsorption process and  $C$  is the concentration of the inhibitors. The obtained slopes, intercepts, and goodness of fit parameters ( $r^2$ ) for CTS, PAA, and CTS-PAA are listed in Table 3. A close look at the fitting plots in Figure 8 and the parameters in Table 3 show that the goodness of fit in all systems approximate unity indicating conformation to Langmuir isotherm. Also, approximate unity slopes indicating minimal interaction in the adsorption layer were obtained in all the systems. Nonetheless, the slight deviation of the slopes from unity can be attributed to the existence of mild interactions between adsorbed species on the surface and/ or changes in the adsorption energies as the surface coverage increases (Njoku *et al.*, 2021c).

The equilibrium constant,  $K_{\text{ads}}$  represents the rate and/or magnitude of adsorption of the adsorbents on the adsorbent. The  $K_{\text{ads}}$  values increase in the modified polymer CTS-PAA compared with PAA and CTS, indicating that the modification enhanced the adsorption capability of the new polymer. These adsorption isotherm parameters confirm that the anticorrosion effects recorded by the various inhibiting agents are due to their adsorption on the steel surface. An interfacial adsorbed film can interrupt the access of water and other corrosive agents as predicted via electrochemical methods.

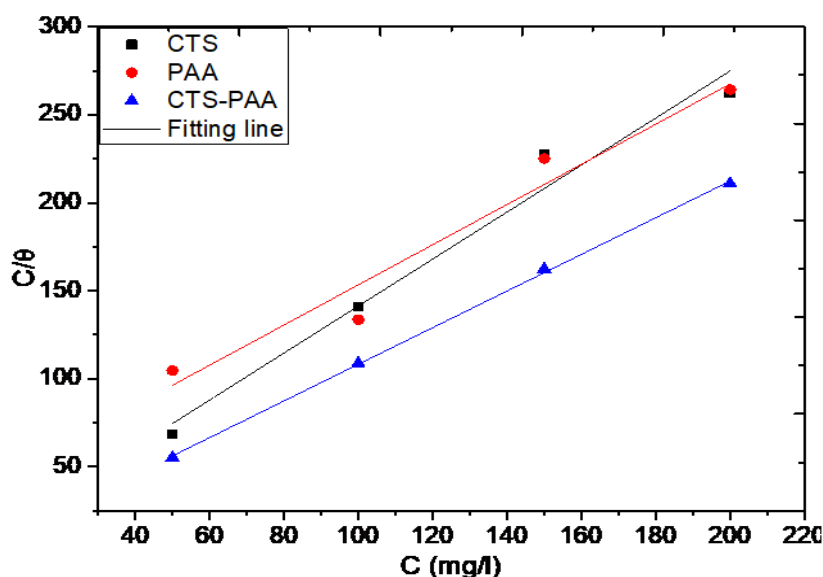


**Figure 8.** Adsorption isotherm plots for the adsorption of CTS, PAA, and CTS -PAA on mild steel in 1 M HCl

### 3.4.2 XPS analysis

XPS analysis comparing the intensities of the chemical states of CTS and CTS-PAA elements on a mild steel surface exposed to 1 M HCl was undertaken to probe the distinct interaction properties of the modified chitosan (CTS-PAA) and CTS. Generally, the steel dissolves by producing  $\text{Fe}^{2+}$  ( $\text{Fe} \rightarrow \text{Fe}^{2+} + 2e^-$ ) which can further oxidize to  $\text{Fe}^{3+}$ . In HCl, chloride ( $\text{Cl}^-$ ) and water molecules ( $\text{H}_2\text{O}$ )<sub>ads</sub> pre-adsorption on the steel surface will produce  $\text{FeCl}_x$  and  $\text{FeOOH}$ . On the other hand, in the presence of organic molecules, the protonation of organic molecules produces ( $-\text{NH}_2^+$ ) while binding energy peaks relating to the adsorption of organic species with steel such as  $\text{Fe}-\text{N}$ ,  $\text{Fe}-\text{NH}_2^+$ ,  $\text{C}=\text{C}/\text{C}=\text{O}$  bonds can be found. Interestingly, with the help of sophisticated XPS analysis, these peaks can be identified to confirm the adoption mechanism. Figure 9 (a-b) presents the XPS data for the interaction of CTS (Figure 9 a) and CTS-PAA, (Figure 9 b) respectively. In both compounds, the deconvolution of the Fe peak produces a binding energy peak at 706.9 eV which is related to the bulk steel ( $\text{Fe}^0$ ). The

peak at 709.2 eV is due to iron (II) state ( $\text{Fe}^{2+}$ ) compounds, while the peak at 710 eV and 713 eV are for iron (III) ( $\text{Fe}^{3+}$ ) state compounds and the associated satellite, respectively (Krishna and Philip, 2022). The O 1s deconvolution peaks at 531.6, 531.8, and 533 eV are assigned to  $\text{O}^{2-}$  (oxides), OH<sup>-</sup> appeared and adsorbed water molecules oxygen (Loto and Loto, 2016; Njoku *et al.*, 2021c).

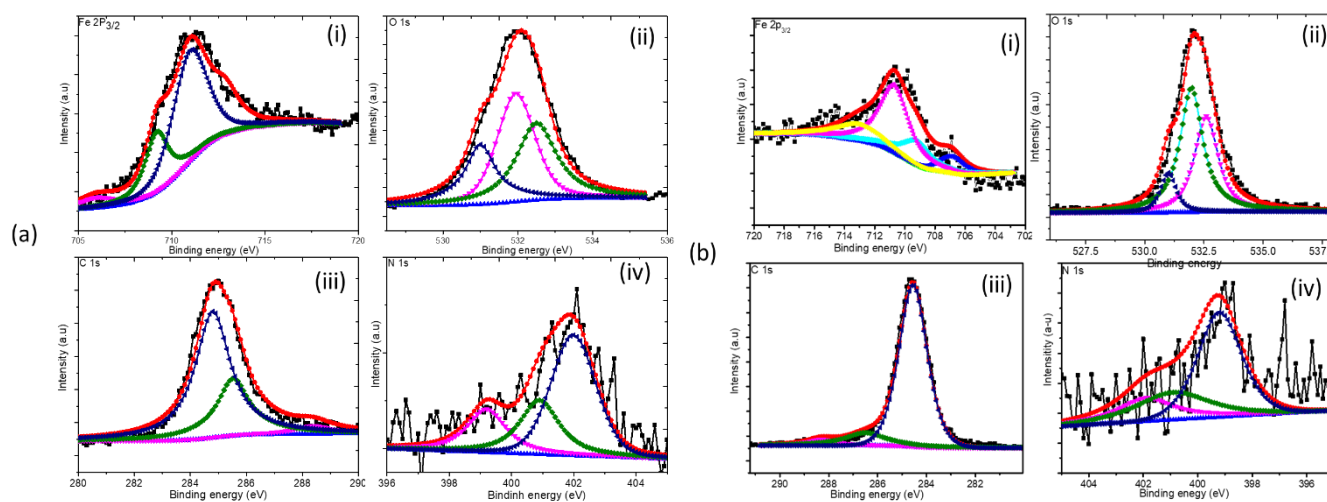


**Figure 9.** The XPS deconvolution peaks for (a) CTS adsorption and (b) CTS-PAA adsorption (i) Fe  $2p_{3/2}$  (ii) O 1s (iii) C 1s and (iv) N 1 s.

The difference between the magnitudes of peaks due to adsorbed water molecules is obvious from the spectrum at 533 eV. CTS-PAA exhibited a 533-eV peak with minimal value for water adsorption compared with the 533-eV peak for CTS. This indicates that the adsorption of the modified compound polymer (CTS-PAA) impacted more compact film with a better hydrophobic effect (evidence of improved adsorption) than CTS which is consistency with the impedance data. Further evidence of the adsorption of organic species on the steel surface can be deduced from the N and C peaks. The peak for N is deconvoluted into binding energy peaks at 399.2 eV, 400.9 eV, and 401.9 eV which are ascribed to C–N, coordinated nitrogen with the steel surface (N-Fe) (Loto and Loto, 2016) and the protonated nitrogen, respectively. Likewise, the carbon (C 1s) peak was deconvoluted into three other peaks belonging to the different structural moieties of the modified polymers. The large peak at 284.5 eV is ascribed to C–C, and C=C or C–H, while the minor peak at 286.4 eV and the non-conspicuous peak at 288.4 eV are related to the carbon atoms bonded with nitrogen in the form of C–N/ C=N and the protonated carbon peak (C=N+), respectively, (Loto and Loto, 2016; Njoku *et al.*, 2021c). Again, upon a comparison of the peak areas, CTS-PAA peaks for both C 1s and N 1s exhibited more peak area values than the CTS peaks. The implication of this is related to enhanced adsorption due to more adsorption centers caused by the PAA grafting in the CTS-PAA. Thus, CTS-PAA adsorbed more than the native CTS which explains the improved inhibition efficiency. The improved adsorption of modified polymers has been speculated previously to enhance interaction/adsorption due to more adsorption sites caused by the modification, but in our report, this has been proved with XPS binding energies of the various elements in the polymers.

### 3.4.3 SEM data

SEM imaging (scanning electron microscopy) provides clear and visible evidence of corrosion protection at the microscopic levels. Excellent corrosion-inhibiting agents will maintain a smooth surface devoid of voids and corrosion products; while weak or poor agents only offer minimized reduction of corrosion products and/or micro defects due to corrosion aggression. However, an

uninhibited system will be laden with both corrosion products and defects indicative of unhindered corrosion action. The images comparing the surface microstructure of the steel exposed in 1 M HCl without and with CTS and CTS-PAA are shown in [Figure 10 \(a-c\)](#). The steel surface exposed in 1 M HCl shows a very rough surface with lots of corrosion products, while the steel surfaces exposed in the systems with CTS and CTS-PAA reveal smooth surfaces devoid of corrosion products which indicates corrosion inhibition action. However, the difference in the corrosion protection ability of CTS-PAA compared with only CTS is obvious which confirms that the modified polymer (CTS-PAA) offered the best protection.

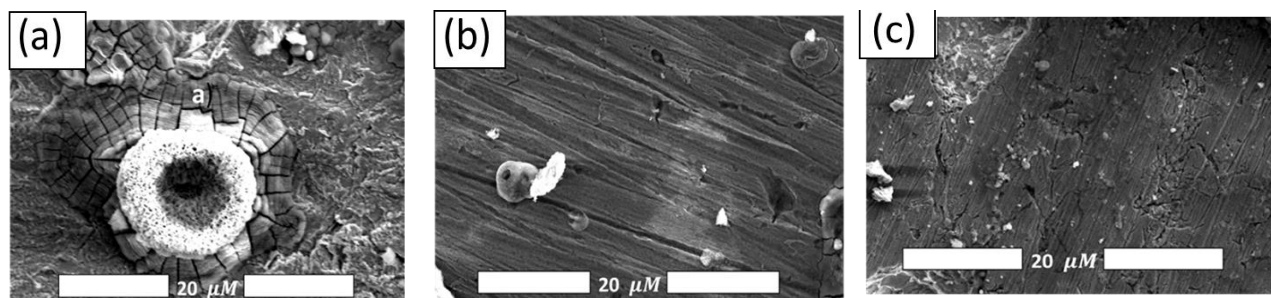


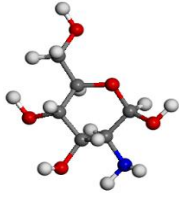
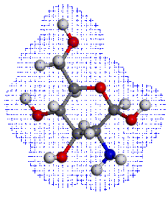
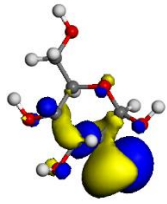
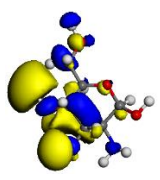
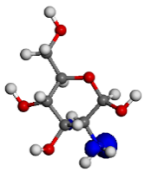
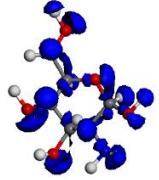
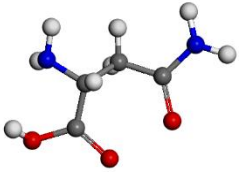
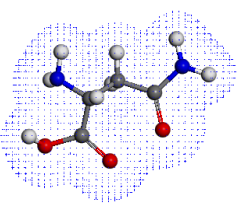
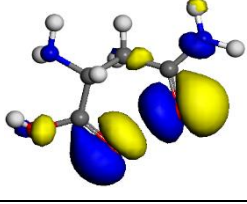
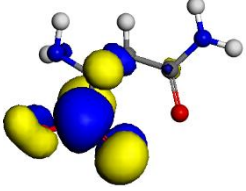
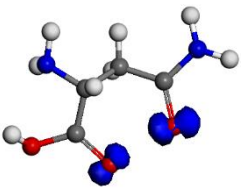
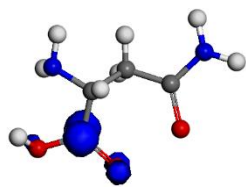
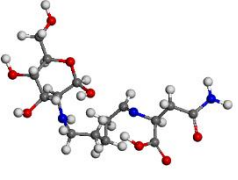
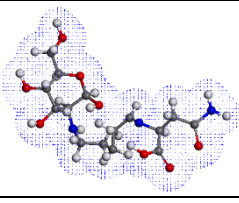
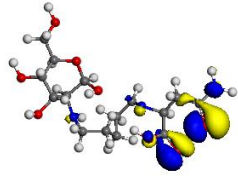
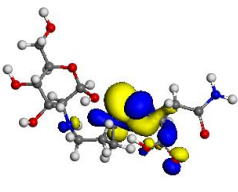
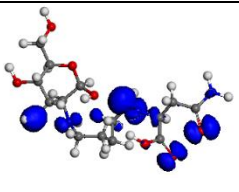
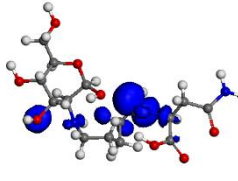
**Figure 10.** SEM images of mild steel in 1 M HCl without (a) and with PAA (b) and CTS-PAA

### 3.5 Theoretical Consideration

#### 3.5.1 Density Functional Theory (DFT)

The DFT computation were carried out herein to ascertain and compare the structural and/or electronic properties of CTS, PAA, and CTS-PAA. The DFT properties have well correlated with their inhibiting capabilities (Singh et al., 2013; Zhang et al., 2016). The interactive adsorption of organic entities on substrates surface is presided over by donor-acceptor reactions. Hence in a molecule, the highest occupied frontier molecular orbital (HOMO) in a compound depicts the electron-donating ability of the organic molecule and the lowest unoccupied frontier molecular orbital (LUMO) which represents the ability of the compound to accept an electron are the two most important indices for predicting the reactivity of a chemical species (Al Hamzi et al., 2013; Emori et al., 2023; Njoku et al., 2018). [Figure 11](#) depicts the representative snapshots revealing the distribution of HOMO and LUMO as well the Fukui reactive centers on CTS, PAA, and CTS-PAA. [Table 4](#) collated the corresponding calculated quantum chemical calculations parameters such as;  $E_{\text{HOMO}}$ ,  $E_{\text{LUMO}}$ ,  $\Delta E$ , and  $\Delta N$ .

The energy difference between the HOMO and the LUMO ( $\Delta E$ ) gives another insight into the reactivity of inhibitor molecules. The energy gap is pertinent to ascertaining the stability index as well as the inhibitors–substrate interaction. Low  $\Delta E$  values, in comparison, can differentiate the inhibition potentials amongst molecules. Small  $\Delta E$  indicate sustainability to enhanced reactivity and polarizable (soft)(Kumar et al., 2013). Close inspection of the data in [Table 4](#), it can be seen that although similar electronic parameters are exhibited by the various compounds, CTS-PAA shows the lowest energy gap value which indicates the optimal disposition to enhanced interaction. Going further,  $\Delta N$  is related to reactivity by the relation:  $\Delta N > 0$ , indicates a high disposition to transfer or release electrons, while  $\Delta N < 0$  indicates a low disposition to transfer or release electrons (Njoku et al., 2018; Oguzie et al., 2014). Positive  $\Delta N$  confirms that the molecules can interact with the steel surface, but the degree will depend on the distinctive polarizability of the compounds ( $\Delta E$ ). The use of Fukui analysis to estimate the adsorption centers of inhibitors has been widely reported (Faska & Majidi, 2018; Iorhuna et al., 2023). In [Figure 11](#) the electron-rich centers ( $f^-$ ) and deficient sites ( $f^+$ ) are revealed by Fukui functions. The modification of CTS with PAA improved the overall electronic properties.

CTS			
	Optimized structure	Total Electron density	HOMO structure
			
	LUMO structure	Electrophilic attack	Nucleophilic attack
PAA			
	Optimized structure	Total Electron density	HOMO structure
			
	LUMO structure	Electrophilic attack	Nucleophilic attack
CTS-PAA			
	Optimized structure	Total Electron density	HOMO structure
			
	LUMO structure	Electrophilic attack	Nucleophilic attack

**Figure 11** DFT results for CTS, PAA and CTS-PAA

### 3.5.2 Molecular dynamics simulation (MDS)

To predict and compare the adsorption strengths of the various compounds on Fe, MDS was carried. This is to probe the distinct interactive strengths of the various tested inhibitor compounds with the steel surface in approximated solution conditions. This section is intended to collaborate the experimental results with theoretical simulation with cognition of the inter-relationship between

metal/adsorbate interaction energies with the corrosion mitigating efficacy propensity (Maduabuchi *et al.*, 2020; Njoku *et al.*, 2019). Table 4 also contains the binding energies of the inhibiting compounds. The higher the binding energies (B.E), the higher the ability of the inhibitors to adsorb firmly and/ or form a compact protective barrier film on the metal surface ( Ben Hmamou *et al.*, 2013; Oguzie *et al.*, 2014). Again, CTS-PAA exhibited higher B.E than both CTS and PAA individual compounds. And the trend of the binding energy values decreases CTS—PAA > CTS > PAA. This is interestingly in perfect agreement with the experimental results and well certify the objective for the synthesis. This shows that the modified compounds will exhibit the best inhibiting efficiency (protective efficacy). The resulting low-energy adsorption structures (side and top views) for the various organic compounds are presented in Figure 12.

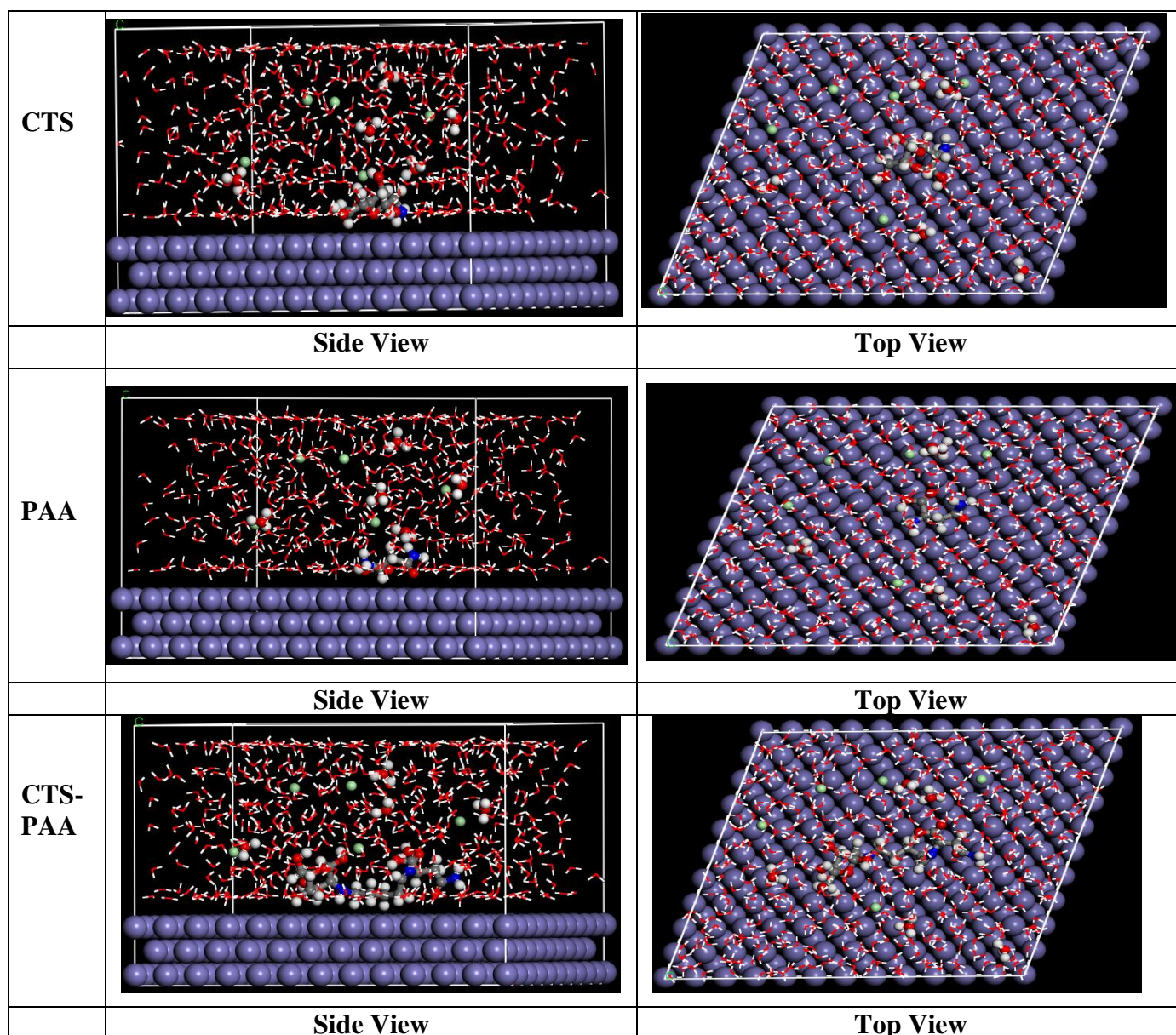


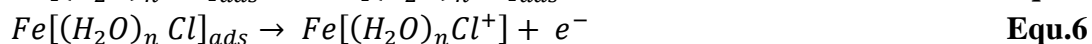
**Figure 12** Top (electrolyte) and side view (gas phase) representations of the lowest energy adsorption configuration of the adsorption of CTS, PAA and CTS-PAA

Interestingly, the compounds adopt a near-flat orientation on the Fe (110) surface. This sort of orientation usually results in the formation of a strong coordinate bond and back-bonding formation between the inhibitor molecules and the Fe (110) surface (Oguzie *et al.*, 2014). From the adsorption configuration of various compounds, it can be seen that the larger compounds (CTS and CTS-PAA)

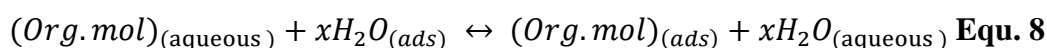
afford better surface coverage of the surface of the metal. High B.E means favourable specific interaction therefore, thus, the modified CTS (CTS-PAA) shows a stronger tendency to adsorb on the steel surface and should provide higher corrosion protection than CTS (Nwanonenyi *et al.*, 2022). Hence, theoretical results support the experimental data.

### 3.6 Inhibition mechanism

Generally, acids corrode steel following ( $\text{Fe} \rightarrow \text{Fe}^{2+} + 2\text{e}^-$ ) making the surface to be positively charged. Therefore, in the presence of chlorides (HCl),  $\text{Cl}^-$  which is negatively charged can be attracted to the surface by electrostatic attraction thereby recharging the steel surface to negatively charge as illustrated in the scheme in Figure 13. Herein the steel corrodes following the notorious equations shown below:



Interestingly, organic molecules protonate at the nitrogen atom of the functional groups as illustrated in the scheme in Figure 13. The implication of these is that electrostatic interaction can provoke the adsorption of these molecules on the steel surface thereby displacing water molecules and other corrosive species according to the model:



Where  $(\text{Org. mol})_{(\text{aqueous})}$  represent organic molecules in solution and  $x\text{H}_2\text{O}_{(\text{ads})}$  represent the previously adsorbed water molecules on the steel surface and vice versa.

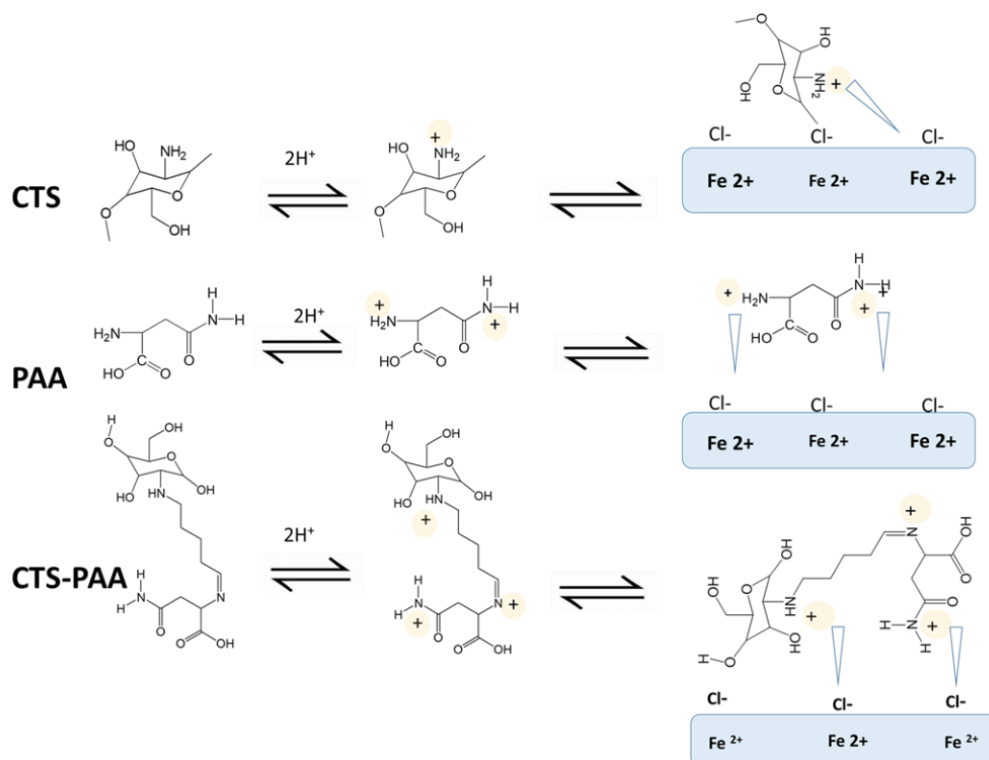


**Figure 13** The protonation and adsorption mechanism of CTS, PAA and CTS-PAA

Hence, the more heteroatoms, the more adsorptive sites. Again, this is the motivation for the grafting of the smaller molecules with additional heteroatom with natural CTS to multiply the number of adsorptive sites in the polymer. As obvious in the scheme describing the mechanism of adsorption of

the various molecules, modification of CTS with PAA via grafting with glutaraldehyde increased the number of adsorptive sites in the new CTS-PAA compound. From the literature, this usually manifests in increased binding and interaction energies of the molecules' adsorption on steel leading to improved corrosion inhibition efficiency. Also, the presence of various adsorption centers (heteroatoms, aromatic rings ...) may introduce a synergistic intramolecular effect (Zhang *et al.*, 2022). The scheme in Figure 13 affords mechanistic insights into the protonation of the inhibitor compounds and their adsorption on the steel surface.

## Conclusions

The experimental data reveal the grafting of CTS with PAA increased the adsorptive centers in the polymer. This manifested in increased adsorption of the CTS-PAA on the steel surface according to the XPS results. The protective effect was duly attributed to the adsorption of the compounds on the steel surface and the adsorption process followed the Langmuir model. Electrochemical data reveal the different effects of the adsorption of CTS, PAA, and the modified polymer – CTS-PAA on steel on the transfer of electrons on the metal/solution interface while polarization data revealed that the adsorbed film exhibited a mixed inhibition mechanism.

SEM data show that in the uninhibited system showed obvious corrosion product compared with the inhibited with the inhibited system; but, CTS-PAA exhibited the most effective protection.

Computational results indicate that the modified compound had the lowest energy gap indicating a better disposition to interact with the steel surface. MDS reveals that the modification led to increased binding energy affirming the DFT electronic data. The overall experiments agree with the computational data in revealing (a) the distinct inhibitive capabilities of PAA, CTS, and CTS-PAA and (b) the merits of the modification.

**Acknowledgement:** The technical inputs of Dr. Demian I. Njoku, of Institute of Metal Research, Chinese Academy of Science, Shenyang, China is acknowledged.

**Disclosure statement:** *Conflict of Interest:* The authors declare that there are no conflicts of interest.

*Compliance with Ethical Standards:* This article does not contain any studies involving human or animal subjects.

## References

- Al Hamzi A. H., Zarrok, H. Zarrouk A., Salghi R., Hammouti B., Al-Deyab S.S., Bouachrine M., Amine A., Guenoun F. (2013), The Role of Acridin-9(10H)-one in the Inhibition of Carbon Steel Corrosion: Thermodynamic, Electrochemical and DFT Studies, *Int. J. Electrochem. Sci.*, 8 N°2, 2586-2605
- Ani, J.U., Obi, I.O., Akpomie, K.G., Eze, S.I., Nwatu, G., (2022). Corrosion Inhibition Studies of Metals in Acid Media by Fibrous Plant Biomass Extracts and Density Functional Theory: A Mini-Review. *J. Nat. Fibers* 19, 2391–2401. [doi.org/10.1080/15440478.2020.1818345](https://doi.org/10.1080/15440478.2020.1818345).
- Auepattana-Aumrung, K., Phakkeeree, T., Crespy, D., (2022). Polymer-corrosion inhibitor conjugates as additives for anticorrosion application. *Prog. Org. Coatings* 163, 106639. <https://doi.org/10.1016/j.porgcoat.2021.106639>.
- Ben Hmamou D., Salghi R., Zarrouk A., Aouad M.R., Benali O., Zarrok H., Messali M., Hammouti B., Ebenso E., Kabanda M.M., Bouachrine M. (2013). Weight loss, electrochemical, quantum chemical calculations and molecular dynamics simulation studies on 2-(benzylthio)-1,4,5-triphenyl-1H-imidazole as inhibitor for carbon steel corrosion in hydrochloric acid, *Ind. Eng. Chem. Res.*, 52 N°40, 14315-14327.
- Beulah Gnana Ananthi, G., Sivakumar, N., Deepak, M.S., (2021). Experimental study of biopolymer in corrosion resistance for industrial exposure condition. *Mater. Today Proc.* 44, 651–658. <https://doi.org/10.1016/j.matpr.2020.10.606>.



- Chai, C., Xu, Yanhua, Xu, Ying, Liu, S., Zhang, L., (2020). Dopamine-modified polyaspartic acid as a green corrosion inhibitor for mild steel in acid solution. *Eur. Polym. J.* 137, 109946. <https://doi.org/10.1016/j.eurpolymj.2020.109946>.
- Chauhan, D.S., Quraishi, M.A., Sorour, A.A., Saha, S.K., Banerjee, P., (2019). Triazole-modified chitosan: A biomacromolecule as a new environmentally benign corrosion inhibitor for carbon steel in a hydrochloric acid solution. *RSC Adv.* 9, 14990–15003. <https://doi.org/10.1039/c9ra00986h>.
- Chen, L., Lu, D., Zhang, Y. (2022). Organic Compounds as Corrosion Inhibitors for Carbon Steel in HCl Solution: A Comprehensive Review. *Mater.* (Basel, Switzerland) 15. [doi.org/10.3390/ma15062023](https://doi.org/10.3390/ma15062023).
- Chen, T., Zeng, D., Zhou, S., (2018). Study of polyaspartic acid and chitosan complex corrosion inhibition and mechanisms. *Polish J. Environ. Stud.* 27, 1441–1448. [doi.org/10.15244/pjoes/78245](https://doi.org/10.15244/pjoes/78245).
- Chopda, L. V, (2023). Small Organic Molecule as Corrosion Inhibitors for Mitigating Metal Corrosion, in: Singh, D.A. (Ed.), *IntechOpen*, Rijeka, p. Ch. 1. [doi.org/10.5772/intechopen.110161](https://doi.org/10.5772/intechopen.110161).
- Dang, N., Wei, Y.H., Hou, L.F., Li, Y.G., Guo, C.L. (2015). Investigation of the inhibition effect of the environmentally friendly inhibitor sodium alginate on magnesium alloy in sodium chloride solution. *Mater. Corros.* 66, 1354–1362. <https://doi.org/10.1002/maco.201408141>.
- El Azzouzi M., Azzaoui K., Warad I., Hammouti B., Shityakov S., Sabbahi R., Saoiabi S., Youssef M.H., Akartasse N., Jodeh S., Lamhamdi A., Zarrouk A. (2022), Moroccan, Mauritania, and Senegalese gum Arabic variants as green corrosion inhibitors for mild steel in HCl: Weight loss, Electrochemical, AFM and XPS studies, *Journal of Molecular Liquids*, 347, 118354, <https://doi.org/10.1016/j.molliq.2021.118354>
- El Mouaden K., El Ibrahim B., Oukhrib R., Bazzi L., Hammouti B., Jbara O., Tara A., Chauhan D. S., Quraishi M.A. (2018). Chitosan polymer as a green corrosion inhibitor for copper in sulfide-containing synthetic seawater, *International Journal of Biological Macromolecules*, 119, 1311–1323
- Elmsellem H., Youssef M. H., Aouniti A., Ben Hadda T., Chetouani A., Hammouti B. (2014), Adsorption and inhibition effect of curcumin on mild steel corrosion in hydrochloric acid, *Russian J. Appl. Chem.*, 87 (6), 744–753
- Emori, W., Louis, H., Okonkwo, P.C., Njoku, D.I., Edet, H.O., Okafor, P.C., Cheng, C.-R., (2023). Dispersive adsorption and anticorrosion properties of natural capsaicin on Q235 steel in mixed H<sub>2</sub>SO<sub>4</sub> and NaCl environment: Characterization, experimental and theoretical studies. *Sustain. Chem. Pharm.* 32, 101042. <https://doi.org/10.1016/j.scp.2023.101042>.
- Erna, M., Herdini, H., Futra, D., (2019). Corrosion Inhibition Mechanism of Mild Steel by Amylose-Acetate/Carboxymethyl Chitosan Composites in Acidic Media. *Int. J. Chem. Eng.* 2019, 8514132. [doi.org/10.1155/2019/8514132](https://doi.org/10.1155/2019/8514132).
- Fardioui, M., Rbaa, M., Benhiba, F., Galai, M., Guedira, T., Lakhrissi, B., Warad, I., Zarrouk, A., (2021). Bioactive corrosion inhibitor based on 8-hydroxyquinoline-grafted-Alginate: Experimental and computational approaches. *J. Mol. Liq.* 323, 114615. <https://doi.org/10.1016/j.molliq.2020.114615>.
- Abu Rub H., Deghles A., Hamed O., Azzaoui K., Hammouti B., Taleb M., Berisha A. Dagdag, O., Mansour, W. Haciosmanoğlu, G. G., Can, Z. S., Rhazi, L. (2023). Cellulose based polyurethane with amino acid functionality: Design, synthesis, computational study and application in wastewater purification, *International Journal of Biological Macromolecules*, 239, 124328, <https://doi.org/10.1016/j.ijbiomac.2023.124328>
- Faska Z., Majidi L. (2018). DFT study on the adsorption mechanism of pulegone and pulegone oxide molecules in gas and aqueous phases as effective corrosion inhibitors in Molar Hydrochloric Acid, *Mor. J. Chem.* 6 N°2 (2018) 283–293
- Fekry A.M., Mohamed R.R. (2010). Acetyl thiourea chitosan as an eco-friendly inhibitor for mild steel in sulphuric acid medium. *Electrochim. Acta* 55, 1933–1939. <https://doi.org/10.1016/j.electacta.2009.11.011>
- Finšgar, M., Jackson, J., (2014). Application of corrosion inhibitors for steels in acidic media for the oil and gas industry: A review. *Corros. Sci.* 86, 17–41. <https://doi.org/10.1016/j.corsci.2014.04.044>.
- Gao, Y., Wang, Y., Liu, Z., Li, H., (2010). Synthesis, scale and corrosion inhibition of modified polyaspartic acid. *Asian J. Chem.* 22, 1495–1502.
- Huang, K., Kong, L., (2013). Preparation and characterization of poly(aspartic acid) derivatives as biodegradable water treatment agents. *Asian J. Chem.* 25, 10233–10237. [doi.org/10.14233/ajchem.2013.15243A](https://doi.org/10.14233/ajchem.2013.15243A).
- Iorhuna F., Ayuba A. M., Thomas N. A. (2023) 2-Phenylpiperazine, N, N'-di-TFA as a corrosion inhibitor: A computational comparative study on the Aluminium and Zinc surface, *Mor. J. Chem.*, 14(3), 884–896.

- Khodair, Z.T., Khadom, A.A., Jasim, H.A., 2019. Corrosion protection of mild steel in different aqueous media via epoxy/nanomaterial coating: preparation, characterization and mathematical views. *J. Mater. Res. Technol.* 8, 424–435. <https://doi.org/10.1016/j.jmrt.2018.03.003>.
- Khoshnaw, F., Gubner, R.B.T.-C.A.C.S. (Eds.) (2022). Part III: Corrosion in Water-Bearing Systems, in: *Corrosion Atlas Series*. Elsevier, pp. lxix–lxxxiv. <https://doi.org/10.1016/B978-0-323-85849-6.02004-7>
- Kong, P., Feng, H., Chen, N., Lu, Y., Li, S., Wang, P. (2019). Polyaniline/chitosan as a corrosion inhibitor for mild steel in acidic medium. *RSC Adv.* 9, 9211–9217. [doi.org/10.1039/C9RA00029A](https://doi.org/10.1039/C9RA00029A).
- Krishna, D.N.G., Philip, J., 2022. Review on surface-characterization applications of X-ray photoelectron spectroscopy (XPS): Recent developments and challenges. *Appl. Surf. Sci. Adv.* 12, 100332. <https://doi.org/10.1016/j.apsadv.2022.100332>.
- Kumar, S., Koh, J., Kim, H., Gupta, M.K., Dutta, P.K., 2012. A new chitosan–thymine conjugate: Synthesis, characterization and biological activity. *Int. J. Biol. Macromol.* 50, 493–502. <https://doi.org/10.1016/j.ijbiomac.2012.01.015>.
- Kumar, S., Sharma, D., Yadav, P., Yadav, M., 2013. Experimental and Quantum Chemical Studies on Corrosion Inhibition Effect of Synthesized Organic Compounds on N80 Steel in Hydrochloric Acid. *Ind. Eng. Chem. Res.* 52, 14019–14029. [doi.org/10.1021/ie401308v](https://doi.org/10.1021/ie401308v).
- Li, L.-F., Celis, J.-P., 2004. Intergranular corrosion of 304 stainless steel pickled in acidic electrolytes. *Scr. Mater.* 51, 949–953. <https://doi.org/10.1016/j.scriptamat.2004.07.022>.
- Lim, S.-H., Hudson, S.M. (2004). Synthesis and antimicrobial activity of a water-soluble chitosan derivative with a fiber-reactive group. *Carbohydr. Res.* 339, 313–319. [doi.org/10.1016/j.carres.2003.10.024](https://doi.org/10.1016/j.carres.2003.10.024).
- Liu, Z., Sun, Y., Zhou, X., Wu, T., Tian, Y., Wang, Y. (2011). Synthesis and scale inhibitor performance of polyaspartic acid. *J. Environ. Sci.* 23, S153–S155. [doi.org/https://doi.org/10.1016/S1001-0742\(11\)61100-5](https://doi.org/10.1016/S1001-0742(11)61100-5).
- Loto, C.A., Loto, R.T. (2016). Corrosion inhibition effect of Allium Cepa extracts on mild steel in H<sub>2</sub>SO<sub>4</sub>. *Der Pharma Chem.* 8, 272–281.
- Maduabuchi, C.A., Njoku, D.I., Anthony, O.I., Nwanonenyi, S.C., Akalezi, C., Blessing, A., Oguzie, E.E. (2020). Experimental and Theoretical Studies on the Protective Effect of a Biomass Corrosion Inhibitor (vignaradiata) on Mild Steel in Acidic Medium. *Electroanalysis* 32, 3117–3130. [doi.org/10.1002/elan.202060378](https://doi.org/10.1002/elan.202060378).
- Melo-Silveira, R.F., Fidelis, G.P., Costa, M.S.S.P., Telles, C.B.S., Dantas-Santos, N., de Oliveira Elias, S., Ribeiro, V.B., Barth, A.L., Macedo, A.J., Leite, E.L., Rocha, H.A.O. (2012). In vitro antioxidant, anticoagulant and antimicrobial activity and in inhibition of cancer cell proliferation by xylan extracted from corn cobs. *Int. J. Mol. Sci.* 13, 409–426. [doi.org/10.3390/ijms13010409](https://doi.org/10.3390/ijms13010409).
- Nascimento, R.C., Furtado, L.B., Guimarães, M.J.O.C. (2023). Biopolymers as Corrosion Inhibitors, in: Grafted Biopolymers as Corrosion Inhibitors. pp. 21–55. <https://doi.org/10.1002/9781119881391.ch3>.
- Natarajan R., Zahir Said Al Shibli F.S. (2021). Synthesis of biomass derived product from Ziziphusspina-christi and application for surface protection of metal under acidic environment- Performance evaluation and thermodynamic studies. *Chemosphere* 284, 131375. [doi.org/10.1016/j.chemosphere.2021.131375](https://doi.org/10.1016/j.chemosphere.2021.131375).
- Njoku, D.I., Li, B., Khan, M.S., Chinonso, U.P., Njoku, C.N., Onyeachu, I.B., Li, Y. (2021a). Quadruple-action coatings provided by doping epoxy with inhibitor laden clay nanotubes functionalized with layer-by-layer of cross-bridged chitosan and anionic polyelectrolytes. *Prog. Org. Coatings* 157, 106312. <https://doi.org/10.1016/j.porgcoat.2021.106312>.
- Njoku, Demian I, Li, Y., Lgaz, H., Oguzie, E.E. (2018). Dispersive adsorption of Xylopiiaethiopica constituents on carbon steel in acid-chloride medium: A combined experimental and theoretical approach. *J. Mol. Liq.* 249, 371–388.
- Njoku, Demian I., Li, Y., Lgaz, H., Oguzie, E.E. (2018). Dispersive adsorption of Xylopiiaethiopica constituents on carbon steel in acid-chloride medium: A combined experimental and theoretical approach. *J. Mol. Liq.* 249, 371–388. [doi.org/10.1016/j.molliq.2017.11.051](https://doi.org/10.1016/j.molliq.2017.11.051).
- Njoku, D.I., Njoku, C.N., Lgaz, H., Okafor, P.C., Oguzie, E.E., Li, Y. (2021b). Corrosion protection of Q235 steel in acidic-chloride media using seed extracts of Piper guineense. *J. Mol. Liq.* 330, 115619. <https://doi.org/10.1016/j.molliq.2021.115619>.
- Njoku, D.I., Okafor, P.C., Lgaz, H., Uwakwe, K.J., Oguzie, E.E., Li, Y. (2021c). Outstanding anticorrosion and adsorption properties of 2-amino-6-methoxybenzothiazole on Q235 and X70 carbon steels: Effect of time, XPS, electrochemical and theoretical considerations. *J. Mol. Liq.* 324, 114663. <https://doi.org/10.1016/j.molliq.2020.114663>.

- Njoku, D.I., Onuoha, G.N., Oguzie, E.E., Oguzie, K.L., Egbedina, A.A., Alshawabkeh, A.N. (2019). Nicotiana tabacum leaf extract protects aluminium alloy AA3003 from acid attack. *Arab. J. Chem.* 12, 4466–4478. <https://doi.org/10.1016/j.arabjc.2016.07.017>.
- Nwanonenyi, S.C., Obasi, H.C., Eze, I.O. (2019). Hydroxypropyl Cellulose as an Efficient Corrosion Inhibitor for Aluminium in Acidic Environments: Experimental and Theoretical Approach. *Chem. Africa* 2, 471–482. [doi.org/10.1007/s42250-019-00062-1](https://doi.org/10.1007/s42250-019-00062-1).
- Nwanonenyi, S.C., Obasi, H.C., Udochukwu, M., Chidiebere, M.A., Njoku, D.I., Oguzie, E. (2022). Protection by a polymer composite on carbon steel surface in 1.0 M HCl environment: a combined experimental and theoretical approach. *Brazilian J. Chem. Eng.* 39, 159–173. [doi.org/10.1007/s43153-021-00187-2](https://doi.org/10.1007/s43153-021-00187-2)
- Oguzie, E.E., Adindu, C.B., Enenebeaku, C.K., Ogukwe, C.E., Chidiebere, M.A., Oguzie, K.L. (2012). Natural products for materials protection: Mechanism of corrosion inhibition of mild steel by acid extracts of piper guineense. *J. Phys. Chem. C* 116, 13603–13615. [doi.org/10.1021/jp300791s](https://doi.org/10.1021/jp300791s).
- Oguzie, Emeka E., Njoku, D.I., Chidebere, M.A., Ogukwe, C.E., Onuoha, G.N., Oguzie, K.L., Ibsi, N. (2014). Characterization and Experimental and Computational Assessment of Kola nitida Extract for Corrosion Inhibiting Efficacy. *Ind. Eng. Chem. Res.* 53, 5886–5894. [doi.org/10.1021/ie404273f](https://doi.org/10.1021/ie404273f).
- Onyeachu, I.B., Njoku, D.I., Nwanonenyi, S.C., Ahanotu, C.C., Etiowo, K.M. (2023). Investigation into the adsorption and inhibition properties of sodium octanoate against CO<sub>2</sub> corrosion of C1018 carbon steel under static and hydrodynamic conditions. *Sci. African* 20, e01603. [doi.org/10.1016/j.sciaf.2023.e01603](https://doi.org/10.1016/j.sciaf.2023.e01603).
- Ouafi A., Hammouti B., Oudda H., Kertit S., Touzani R., Ramdani A. (2002), New pyrazole derivatives as effective Inhibitors for the corrosion of mild steel in HCl medium, *Anti-Corros. Meth. Mater.* 49 N°3, 199-204. <https://doi.org/10.1108/00035590210426463>
- Ouici, H.B., Benali, O., Guendouzi, A., (2016). Experimental and quantum chemical studies on the corrosion inhibition effect of synthesized pyrazole derivatives on mild steel in hydrochloric acid. *Res. Chem. Intermed.* 42, 7085–7109. [doi.org/10.1007/s11164-016-2520-0](https://doi.org/10.1007/s11164-016-2520-0).
- Queiroz, M.F., Melo, K.R.T., Sabry, D.A., Sasaki, G.L., Rocha, H.A.O., (2015). Does the use of chitosan contribute to oxalate kidney stone formation? *Mar. Drugs* 13, 141–158. [doi.org/10.3390/md13010141](https://doi.org/10.3390/md13010141).
- Saha, S.K., Dutta, A., Ghosh, P., Sukul, D., Banerjee, P., (2016). Novel Schiff-base molecules as efficient corrosion inhibitors for mild steel surface in 1 M HCl medium: Experimental and theoretical approach. *Phys. Chem. Chem. Phys.* 18, 17898–17911. [doi.org/10.1039/c6cp01993e](https://doi.org/10.1039/c6cp01993e).
- Sangeetha, Y., Meenakshi, S., SairamSundaram, C., (2015). Corrosion mitigation of N-(2-hydroxy-3-trimethyl ammonium)propyl chitosan chloride as inhibitor on mild steel. *Int. J. Biol. Macromol.* 72, 1244–1249. <https://doi.org/10.1016/j.ijbiomac.2014.10.044>.
- Shahini, M.H., Ramezanzadeh, B., Mohammadloo, H.E., (2021). Recent advances in biopolymers/carbohydrate polymers as effective corrosion inhibitive macro-molecules: A review study from experimental and theoretical views. *J. Mol. Liq.* 325, 115110. <https://doi.org/10.1016/j.molliq.2020.115110>.
- Shanmugapriya, R., Ravi, M., Ravi, S., Ramasamy, M., Maruthapillai, A., J, A.S., (2023). Electrochemical and Morphological investigations of Elettaria cardamomum pod extract as a green corrosion inhibitor for Mild steel corrosion in 1 N HCl. *Inorg. Chem. Commun.* 154, 110958. <https://doi.org/10.1016/j.inoche.2023.110958>.
- Silva, F.R.F., Dore, C.M.P.G., Marques, C.T., Nascimento, M.S., Benevides, N.M.B., Rocha, H.A.O., Chavante, S.F., Leite, E.L., (2010). Anticoagulant activity, paw edema and pleurisy induced carrageenan: Action of major types of commercial carrageenans. *Carbohydr. Polym.* 79, 26–33. <https://doi.org/10.1016/j.carbpol.2009.07.010>.
- Singh, R.N., Kumar, A., Tiwari, R.K., Rawat, P., (2013). A combined experimental and theoretical (DFT and AIM) studies on synthesis, molecular structure, spectroscopic properties and multiple interactions analysis in a novel Ethyl-4-[2-(thiocarbamoyl)hydrazinylidene]-3,5-dimethyl-1H-pyrrole-2-carboxylate and it. *Spectrochim. Acta Part A Mol. Biomol. Spectrosc.* 112, 182–190. <https://doi.org/10.1016/j.saa.2013.04.002>
- Song, C., Yu, H., Zhang, M., Yang, Y., Zhang, G., (2013). Physicochemical properties and antioxidant activity of chitosan from the blowfly *Chrysomyamegacephala* larvae. *Int. J. Biol. Macromol.* 60, 347–354. [doi.org/10.1016/j.ijbiomac.2013.05.039](https://doi.org/10.1016/j.ijbiomac.2013.05.039).
- Speight, J.G., (2014). Chapter 2 - Mechanism of Acid Corrosion, in: Speight, J.G.B.T.-H.A.C. (Ed.) *Gulf Professional Publishing, Boston*, pp. 31–55. <https://doi.org/10.1016/B978-0-12-800630-6.00002-2>.
- Sweetman, A., (2020). A Grand Challenge for Environmental Organic Chemistry: How Can We Avoid Regrettable Substitution? *Front. Environ. Chem.* 1 [doi.org/10.3389/fenvc.2020.00007](https://doi.org/10.3389/fenvc.2020.00007).

- Umoren, S.A., AlAhmary, A.A., Gasem, Z.M., Solomon, M.M., 2018. Evaluation of chitosan and carboxymethyl cellulose as ecofriendly corrosion inhibitors for steel. *Int. J. Biol. Macromol.* 117, 1017–1028. <https://doi.org/10.1016/j.ijbiomac.2018.06.014>.
- Vaghefinazari, B., Wierzbicka, E., Visser, P., Posner, R., Arrabal, R., Matykina, E., Mohedano, M., Blawert, C., Zheludkevich, M.L., Lamaka, S. V., 2022. Chromate-Free Corrosion Protection Strategies for Magnesium Alloys—A Review: Part III—Corrosion Inhibitors and Combining Them with Other *Protection Strategies. Materials* (Basel). 15. [doi.org/10.3390/ma15238489](https://doi.org/10.3390/ma15238489).
- Verma, C., Kumar, A.M., Mazumder, M.A.J., Quraishi, M.A. (2018). Chitosan-Based Green and Sustainable Corrosion Inhibitors for Carbon Steel, in: Dongre, R.S. (Ed.), *IntechOpen*, Rijeka, p. Ch. 8. [doi.org/10.5772/intechopen.74989](https://doi.org/10.5772/intechopen.74989).
- Verma, C., Quraishi, M.A. (2021). Chelation capability of chitosan and chitosan derivatives: Recent developments in sustainable corrosion inhibition and metal decontamination applications. *Curr. Res. Green Sustain. Chem.* 4, 100184. <https://doi.org/10.1016/j.crgsc.2021.100184>.
- Verma, C., Quraishi, M.A., Kluza, K., Makowska-Janusik, M., Olasunkanmi, L.O., Ebenso, E.E. (2017). Corrosion inhibition of mild steel in 1M HCl by D-glucose derivatives of dihydropyrido [2,3-d:6,5-d'] dipyrimidine-2, 4, 6, 8(1H,3H, 5H,7H)-tetraone. *Sci. Rep.* 7, 44432. [doi.org/10.1038/srep44432](https://doi.org/10.1038/srep44432).
- Verma, C., Quraishi, M.A., Rhee, K.Y. (2022). Aqueous phase polymeric corrosion inhibitors: Recent advancements and future opportunities. *J. Mol. Liq.* 348, 118387. <https://doi.org/10.1016/j.molliq.2021.118387>.
- Vino, A.B., Ramasamy, P., Shanmugam, V., Shanmugam, A. (2012). Extraction, characterization and in vitro antioxidative potential of chitosan and sulfated chitosan from Cuttlebone of Sepia aculeataOrbigny, 1848. *Asian Pac. J. Trop. Biomed.* 2, S334–S341. [https://doi.org/10.1016/S2221-1691\(12\)60184-1](https://doi.org/10.1016/S2221-1691(12)60184-1).
- Wang, Y., Wang, J., Yuan, Z., Han, H., Li, T., Li, L., Guo, X. (2017). Chitosan cross-linked poly(acrylic acid) hydrogels: Drug release control and mechanism. *Colloids Surf. B. Biointerfaces* 152, 252–259. [doi.org/10.1016/j.colsurfb.2017.01.008](https://doi.org/10.1016/j.colsurfb.2017.01.008).
- Wang, Z., Cai, Z., Han, X., Zhang, H., Shao, Z., Xiao, K., Fan, Y., Wang S. (2023). Influence of sodium alginate and chromate on aluminum corrosion in simulated HVDC cooling water. *Int. J. Electrochem. Sci.* 18, 100073. [doi.org/https://doi.org/10.1016/j.ijoes.2023.100073](https://doi.org/10.1016/j.ijoes.2023.100073).
- Wei, H., Heidarshenas, B., Zhou, L., Hussain, G., Li, Q., Ostrikov, K. (Ken), (2020). Green inhibitors for steel corrosion in acidic environment: state of art. *Mater. Today Sustain.* 10, 100044. [doi.org/https://doi.org/10.1016/j.mtsust.2020.100044](https://doi.org/10.1016/j.mtsust.2020.100044).
- Wolkers, W.F., Oliver, A.E., Tablin F., Crowe J.H. (2004). A Fourier-transform infrared spectroscopy study of sugar glasses. *Carbohydr. Res.* 339, 1077–1085. [doi.org/https://doi.org/10.1016/j.carres.2004.01.016](https://doi.org/10.1016/j.carres.2004.01.016)
- Yaagoob, I.Y., Goni, L.K.M.O., Mazumder, M.A.J., Ali, S.A., Alfantazi, A., Verma, C. (2023). Surface and interfacial properties of poly(methylallylammonium chloride): Effect of hydrophobic pendant and synergism (KI) on corrosion of C1018CS in 15% HCl. *J. Taiwan Inst. Chem. Eng.* 149, 105000. [doi.org/https://doi.org/10.1016/j.jtice.2023.105000](https://doi.org/10.1016/j.jtice.2023.105000).
- Yihang, Z., 2022. Application of water-soluble polymer inhibitor in metal corrosion protection: *Progress and challenges. Front. Energy Res.* 10. [doi.org/10.3389/fenrg.2022.997107](https://doi.org/10.3389/fenrg.2022.997107).
- Zhang, Z., Tian, N.C., Huang, X.D., Shang, W., Wu, L. (2016). Synergistic inhibition of carbon steel corrosion in 0.5 M HCl solution by indigo carmine and some cationic organic compounds: experimental and theoretical studies. *RSC Adv.* 6, 22250–22268. [doi.org/10.1039/C5RA25359D](https://doi.org/10.1039/C5RA25359D).
- Zhang Q.H., Jiang Z.N., Li Y.Y., Wang X., Xiong W., H.F. Liu, Zhang G.A. (2022). In-depth insight into the inhibition mechanism of the modified and combined amino acids corrosion inhibitors: “intramolecular synergism” vs. “intermolecular synergism”, *Chemical Engineering Journal*, 437, Part 2, 135439, ISSN 1385-8947, <https://doi.org/10.1016/j.cej.2022.135439>
- Zhou, Z., Zheng, B., Lang H., Qin A., Ou J. (2020). Corrosion resistance and biocompatibility of polydopamine/hyaluronic acid composite coating on AZ31 magnesium alloy. *Surfaces and Interfaces* 20, 100560. [doi.org/https://doi.org/10.1016/j.surfin.2020.100560](https://doi.org/10.1016/j.surfin.2020.100560)

---

(2023); <https://revues.imist.ma/index.php/morjchem/index>